Materials Science & Engineering A 707 (2017) 576–584

Contents lists available at ScienceDirect

Materials Science & Engineering A

journal homepage: www.elsevier.com/locate/msea

Origin of the Bauschinger effect in a polycrystalline material

A.A. Mamun[a,*], R.J. Moat[a], Joe Kelleher[b], P.J. Bouchard[a]

[a] Engineering and Innovation, The Open University, Milton Keynes MK7 6AA, UK
[b] ISIS Facility, Rutherford Appleton Laboratory, Didcot, Oxford OX11 0QX, UK

ARTICLE INFO

Keywords:
Bauschinger effect
Kinematic hardening
Neutron diffraction
Residual strains
Stainless steel

ABSTRACT

There is a long and lively debate in the literature about the origin of the Bauschinger effect in polycrystalline materials, the most widely accepted explanation being the easier movement of dislocations during reverse loading causing the reduction of the yield stress. Other explanations include incompatible deformation at the grain scale and change of dislocation cell structures during forward and reverse loading, but recent publications show these phenomenological explanations of the Bauschinger effect are not holistic. In the experimental work presented here, we have investigated the role of micro residual lattice strain on the origin of the Bauschinger effect in type 316H austenitic stainless steel using in-situ neutron diffraction. Standard cylindrical specimens were tension-compression load cycled at room temperature with the loading interrupted at incrementally larger compressive and tensile strains followed by reloading to the tensile loop peak strain. Mirror symmetric cyclic tests were also performed with tensile and compressive load interruptions followed by compressive reloading to the compressive loop peak strain. A strong correlation is demonstrated between the evolution of residual lattice strain in the grain families and the change in magnitude in macroscopic yield stress, peak stress and the shape of the yielding part of the stress-strain curve for both the cyclic tension yield and compression yield tests. This implies that the residual lattice strain generated by grain scale elastic and plastic deformation anisotropy is the primary source of the Bauschinger kinematic hardening effect observed in type 316H austenitic stainless steel.

1. Introduction

Kinematic hardening of steel during tension-compression cyclic loading was first described by Bauschinger [1] in 1886. In his paper he established the following two laws [2]:

- If a bar is loaded beyond its elastic limit, this increases the elastic limit of the bar for a subsequent load in the same direction.
- Plastically deforming a bar in tension or compression reduces the elastic limit of the bar for a subsequent compression or tension loading respectively. The more the bar has deformed plastically the greater the reduction in the reverse loading elastic limit.

The Bauschinger effect can significantly affect the deformation response of materials and structures which experience tension-compression cyclic loading, by altering the material's elastic limit during the reverse cycle. Such effects can, therefore, be important for life estimation of metallic components in practical applications, for example, power generation plant components. Inelastic constitutive models (for example [3]), are usually used to predict the evolution of stress-strain during such cyclic loading. Such models often use Bauschinger tests as means for characterising work hardening in the material. Therefore in order to develop an accurate inelastic constitutive model for a material it is critical to understand the mechanisms controlling the Bauschinger effect.

The Bauschinger effect has been observed in many single crystal and polycrystalline metallic materials including aluminium [4], nickel [5], steel [6,7], copper and brass [8]. Many investigations have been conducted exploring the origin of the observed Bauschinger effect in these and other metals. However, the number of models or theories that have been developed to explain the Bauschinger effect is almost equal to the number of investigations [9]. The theories can be divided into two overarching groups; continuum and microstructure based. Generally speaking, continuum theories describe the Bauschinger effect in terms of back stresses, generated due to inhomogeneous deformation in the material, while microstructure based theories describe it in terms of dislocation structures and those interactions with other dislocations, precipitates etc. in the material's microstructure during forward and reverse loading.

The most accepted microstructure based explanation for the Bauschinger effect of Orowan [10] and Sleeswyk [11] describes the mechanism in terms of easier reversibility of dislocation motion upon

* Corresponding author.
E-mail addresses: Abdullah.mamun@open.ac.uk, mamun1279xbcc@gmail.com (A.A. Mamun).

http://dx.doi.org/10.1016/j.msea.2017.09.091
Received 7 August 2017; Received in revised form 18 September 2017; Accepted 20 September 2017
Available online 21 September 2017

load reversal. Among notable theories, Mughrabi [12] proposed that incompatibility of deformation between harder cell walls and softer cell interiors of dislocation cell type structures caused the Bauschinger effect. It is well evidenced that formation of dislocation cell type structures induces internal stress in the material [13–15], and a number of investigations [12,16–18] have been conducted correlating such stresses with the Bauschinger effect. Moreover, a number of semi-phenomenological theories [16,18–26] have described the correlation between the changes in dislocation structures during reverse loading and the material's hardening behaviour. These models postulate formation of dislocation structures and dissolution of the structures during reverse loading as the primary cause of the Bauschinger effect in metals. However, such theories of dislocation cell type structures in polycrystalline materials have been contradicted by others, for example [20,27,28,29,30,31]. In the light of these recent publications, it can be stated that dislocation cell type structures and changes of these structures during the cyclic loading direction change have no unique relationship with the observed Bauschinger effect.

Recently, the contribution of residual lattice stress (also termed type II residual stress, intergranular stress, internal stress, micro residual stress and misfit stress) to the Bauschinger effect has been discussed [32,33,34]. Lattice residual stress/strain originates due to a combination of elastic and plastic anisotropy of deformation at the grain scale. Its potential role in the kinematic hardening of metals was predicted a long time ago [35,36]. However, there is little published experimental evidence characterising the relationship between micro residual stress and observed macroscopic deformation in polycrystalline materials.

In this paper, we present results from a set of uniaxial cyclic stress-strain tests which investigate the relationship between the evolution of internal lattice residual strains and observed macroscopic Bauschinger effect in AISI Type 316H austenitic stainless steel at room temperature. In-situ neutron diffraction is used to measure the evolution of residual strains in variously oriented crystallographic grain families after being interrupted at various points in the forward loading cycle and correlating these residual strains with the observed change in macroscopic yield stress during the following reverse and forward loading cycle. We believe this is the first time that a direct correlation between micro residual strain and the Bauschinger effect has been quantified experimentally.

2. Material and experimental technique

The cyclic stress-strain specimens for the experiment were machined from as-received AISI type 316H austenitic stainless steel bar and then solution heat-treated (1050 °C heat soak for 1 h followed by a water quench). The cylindrical test specimens had a gauge diameter of 8 mm, a gauge length of 14 mm and a total length of 74 mm.

Lattice strain measurement using neutron diffraction is a well-established technique [37]. For the present study, in-situ neutron diffraction was used to measure the evolution of lattice strains during cyclic deformation. The experiment was conducted using the Engin-X Time of Flight (ToF) neutron diffraction instrument [38] at the Rutherford Appleton Laboratory, UK. The ToF technique allows the change of lattice spacing between crystallographic planes to be measured for variously oriented grain families simultaneously. The measured spacings are then converted to elastic lattice strain values for specific grain families. The Engin-X instrument is equipped with a stress-rig for in-situ experiments which allowed measurement of the evolution of lattice strains as a function of applied load and strain path. A neutron gauge volume of $4 \times 6 \times 4\ mm^3$ was used with an average neutron counting time of ~ 300 s per measurement point. The macroscopic strain was measured using an Instron extensometer placed in the gauge length of the specimen.

3. Experimental plan

The aim of the first test was to investigate the changes in cyclic tension yield stress with respect to various load interruptions in tension and compression, hence this experiment is denoted 'tension yield test'. The aim of the second test was to investigate the changes in cyclic compression yield stress again with respect to various load interruptions in tension and compression interruptions, accordingly, this second experiment is denoted 'compression yield test'.

First, a type 316H austenitic stainless steel specimen was subjected to a small stabilising load (5 MPa stress) and the reference lattice spacing (d_0) between lattice planes measured for a number of crystallographic grain families. A grain family consists of a set of grains with similar crystallographic orientation, of which the corresponding *hkl* plane normal lies parallel to the scattering vector of the diffraction. The specimen was then subjected to continuous tension-compression cyclic loading, starting in tension, with a strain rate of $7 \times 10^{-6}\ s^{-1}$ over a total strain range of ± 1% up to the point of saturation of cyclic isotropic work hardening in the material. Upon reaching an isotopically saturated work hardened stage, the loading of the specimen was interrupted at various tensile and compressive strains, such that, a pronounced Bauschinger effect was observed in the material's yielding behaviour during reloading cycles. The interruption strains were chosen systematically at an interval of 0.2% strain. The interruption points of

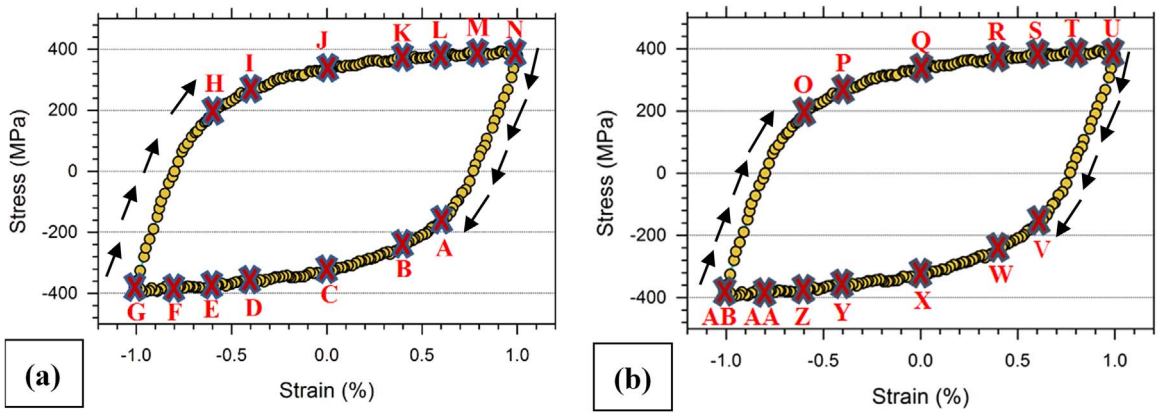

Fig. 1. (a) Interruption points for tension yield test and (b) compression yield test shown in a typical saturated cyclic stress-strain curve of type 316H stainless steel. In (a), points A–G were interrupted while going into compression from a tensile peak strain of 1%. The specimen was reloaded to tensile peak strain after these interruptions. Points H–N were interrupted while going into tension from a compressive peak strain of − 1%. The specimen was unloaded to near zero stress (~ 5 MPa) and reloaded back to tensile peak strain of 1% after these interruptions. In (b), points O–U were interrupted while going into tension from a compressive peak strain of − 1%. The specimen was unloaded to compressive peak strain after these interruptions. Points V–AB were interrupted while going into compression from a tensile peak strain of 1%. The specimen was unloaded to near zero stress (~ 5 MPa) and reloaded to compressive peak strain of − 1% after these interruptions. The black arrows show the direction of loading.

the tension yield test and the compression yield test are shown in Fig. 1(a) and (b) respectively. A few interruption points were skipped in the middle because of the limited neutron experiment beam time available.

After interruption at any point, the specimen was elastically unloaded or reloaded to 5 MPa stress from tension and compression respectively. The elastic lattice strains in at least 5 grain families were measured at this stabilised "unloaded" state. This allowed the measurement of residual lattice strains corresponding to the interruption points in the cycle. Following this measurement, the specimen was reloaded to the tension peak strain (1%) for the tension yield test and compression peak strain (− 1%) for the compression yield test. The residual lattice strains were also measured at the peak cyclic strain positions by unloading from the peak strain to 5 MPa in the next cycle. The macroscopic yield stress was measured for the reloading cycle after any interruptions, at a strain offset of 0.05%. This level offset of strain, which is smaller than the 0.2% or 1% levels conventionally used for defining yielding proof stress, was deliberately chosen to measure more precisely the effect of the residual lattice strain on the initiation of macroscopic yielding. In between each interrupted cycle, at least 2 full cycles were performed to return the specimen to the isotopically saturated hardened state.

4. Tension yield test

4.1. Role of residual lattice strain on macroscopic yielding

Fig. 2 shows the tension yield test macroscopic deformation curves during tension-compression cyclic loading with interruptions at various strains under compressive and tensile loading respectively. The tensile yield stress in the reloading cycle is observed to systematically decrease with the increase of interruption strain in compression. Conversely, the tensile yield stress was found to systematically increase with the increase of interruption strain in tension. In other words, the results first show that the further the elastic limit is exceeded in the compressive direction, the lower the yield stress in the subsequent tension reloading cycle, and secondly the further the elastic limit is exceeded in the tensile direction, the higher the yield stress in the subsequent tension reloading cycle. The measured tensile yield stresses with respect to various compression and tension interruption strains are shown in Table 1 and presented in Fig. 3.

The yield stresses show a large variation with respect to interruption strains. The range of variation in yield after compression and tension interruptions is similar (194 MPa and 188 MPa). The monotonic tensile yield stress of undeformed type 316H stainless steel at 0.05% strain offset is 179 MPa [39]. It is evident that for the case of tension interruptions, the macroscopic yield stress is always higher than the undeformed yield stress and for the case of compression interruptions, the yield stress is less than the undeformed material for small compressive deformation excursions and greater for large compressive excursions.

Lattice strains of at least five grain families parallel to the loading axis (axial) and transverse to it were recorded in the unloaded state. Results for the axial direction alone are presented in this paper. Strains

Table 1
Measured yield at 0.0005 strain offset in the reloading cycle after load interruption at various points in compression and tension loading for the tension yield test. The points of interruption are referred to in Fig. 1.

Compression interruption points	**A**	**B**	**C**	**D**	**E**	**F**	**G**
Interruption strain (%)	0.60	0.40	0.0	−0.40	−0.60	−0.80	−1.0
Yield at 0.05% strain offset (MPa)	282	225	155	118	110	100	88
Tension interruption points	**H**	**I**	**J**	**K**	**L**	**M**	**N**
Interruption strain (%)	− 0.60	− 0.40	0.0	0.40	0.60	0.80	1.0
Yield at 0.05% strain offset (MPa)	210	275	338	372	384	392	398

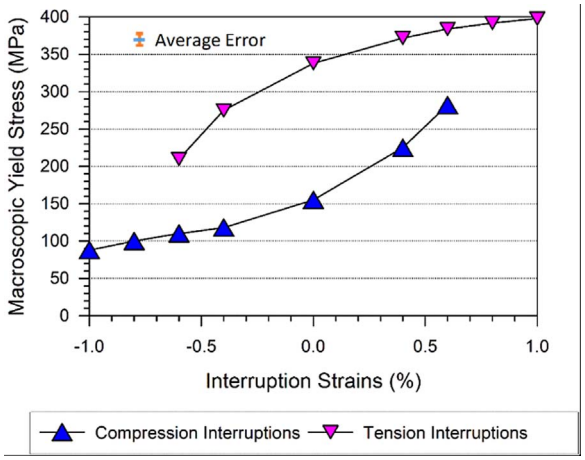

Fig. 3. Changes of cyclic tensile yield stress at 0.05% strain offset after reloading from various tensile and compressive load interruptions. The yield stresses decrease with increasing interruption in compressive load and increase with increasing interruption in tensile load.

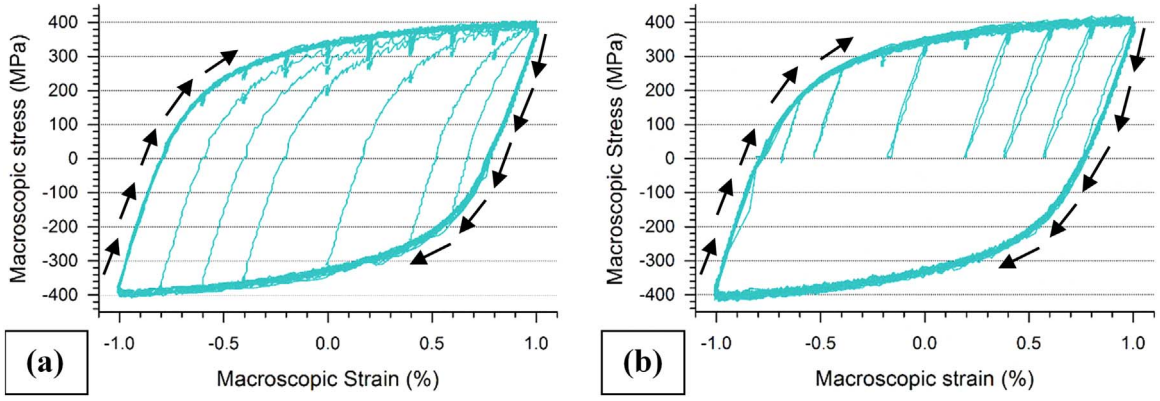

Fig. 2. Macroscopic stress-strain curves for the tension yield test showing interruptions in loading and variation of the shape and magnitude of yielding in the reloading cycle after these interruptions. After each interruption, the load was reduced and increased to 5 MPa for (a) compression and (b) tension interruptions followed by reloading to 1% tensile peak strain. The black arrows show the direction of loading.

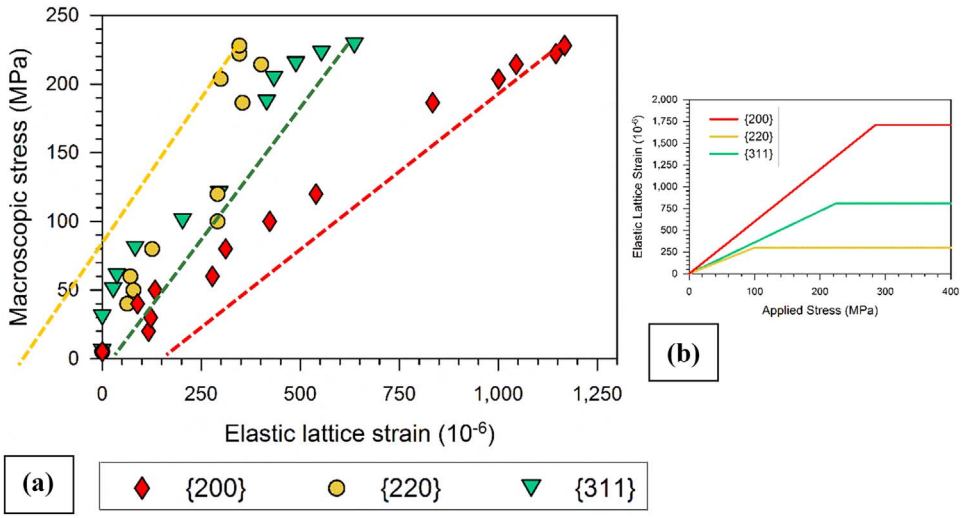

Fig. 4. (a) Evolution of axial elastic lattice strain in 3 grain families during a tensile test of type 316H austenitic stainless steel at room temperature. It can be observed that, with increasing applied stress, the elastic lattice strains in the {220} grain family stopped increasing at an applied stress of ~ 100 MPa, implying grains belonging to this family have started to deform plastically at that point, while the grains of the other two families are still deforming elastically. (b) Schematic plot showing relative yielding of the 3 grain families with increasing applied stress.

measured by neutron diffraction in the loading direction are more reliable than for transverse directions [40–42] owing to higher uncertainty regarding the exact grain population being sampled in the latter.

Investigating the lattice strains of the grain families covering the full spectrum of anisotropy is sufficient to provide a complete insight of the microscopic deformation mechanisms [42]. During uniaxial tensile/compressive deformation of undeformed type 316H stainless steel, the {220} grain family usually yields first, the {200} grain family last and the {311} grain family generally exhibits grain average behaviour [42]. Results from these three grain families alone are presented and discussed in the remainder of this paper as they represent the behaviours of plastically weaker, stronger and average grains in type 316H austenitic stainless steel.

Before presenting the neutron diffraction measurements during cyclic loading, the mechanism by which residual lattice strains are generated is described. Fig. 4 shows the deformation of three differently oriented grain families during a room temperature tensile test of type

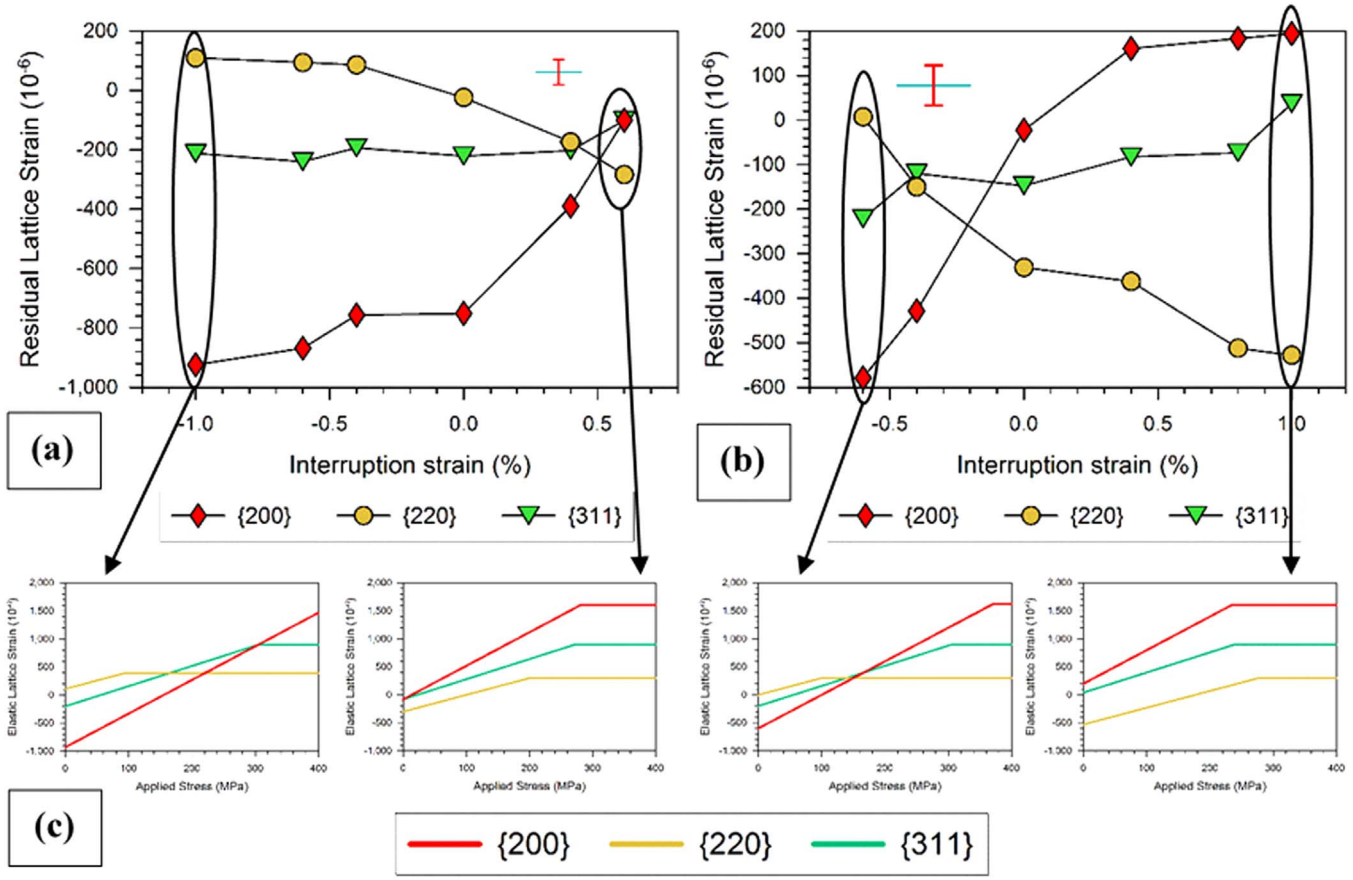

Fig. 5. Axial residual lattice strains at 5 MPa after the interruption at various strains during (a) compressive loading (points A–G in Fig. 1) and (b) during tensile loading (Point H–N in Fig. 1). (c) Schematics showing how the residual strains in the grain families at the 4 extreme points (as circled in (a) and (b) of the figure) changes the order in which the yielding occurs first as well as how that determines the applied stress at which macroscopic yielding initiates. Moreover, the schematic shows how the difference between the yield stresses of different grain families is varied owing to the residual strains which change the shape of elastic to plastic transition of the macroscopic stress-strain curve, as discussed later in this paper.

316H stainless steel. It can be observed that with increasing applied stress the grain families elastically deform with different slopes depending upon the orientation-specific crystallographic elastic modulus. More interestingly, with increasing applied stress, the elastic lattice strains in the {220} grain family can be observed to almost stop increasing at an applied stress of ~ 100 MPa whereas lattice strains in the other two grain families are still increasing. As 'elastic' strains are measured by diffraction, this observation implies that the {220} grain families have already started to deform plastically at that point of loading while the other two grain families are still deforming elastically. Residual lattice strains are generated by this incompatibility of elastic and plastic deformation among differently oriented grains. For example, if the material is elastically unloaded from the peak strain of this tensile test, the grain families will unload following their respective elastic moduli and therefore, the plastically weaker {220} grain family will end up in compressive residual strain while that of the {200} grain family will end up in tensile residual strain, as shown by the dotted line in Fig. 4(a). These residual strains will either assist or oppose yielding during reverse cycle loading depending upon the direction of the reloading. Fig. 4(b) is a schematic diagram illustrating relative yielding of the grain families during a tensile test.

Fig. 5 shows the axial residual lattice strains measured at the unloaded state (at 5 MPa) after various (a) compression and (b) tension interruptions. In case of compressive interruptions, with the increase of interruption strain, the residual lattice strains in the {200} and {220} grain families show a systematic increase in compression and tension directions respectively. In case of the tension interruptions, with an increase of interruption strains, the residual lattice strains in the {200} and {220} grain families show a systematic increase in opposite direction that is to tension and compression directions respectively. In both cases, the lattice strains in the {311} grain family remain nearly unchanged irrespective of the interruption strains, apart from a few points.

Yielding of polycrystalline material initiates by slip occurring in the grains which are favourably oriented, rather than slip occurring in all the grains simultaneously. As the grains belonging to the {220} grain family are the plastically weaker grains, initiation of macroscopic yielding in this material is dictated by the residual strain in this grain family, as it can be seen from the sketches in Fig. 5(c) that in almost all scenarios of interruption (except after 1% tensile interruption), the {220} grain family is the first to yield. Tensile residual strains that develop in the {220} grain families during loading will assist and the compressive residual strains will oppose yielding in the reloading tensile cycle. As shown in Fig. 5(a), the higher the compressive interruption strains, the higher the tensile residual strain in the {220} grain families, and therefore, the lower will be the macroscopic tensile yield stress in the reloading cycle, which is exactly what has been observed in Fig. 3.

To further clarify notice that the {220} grain family possesses a compressive residual strain of ~ 300 με and tensile residual strain of ~ 100 με, in Fig. 5(a), after unloading from interruption at 0.6% strain and at − 0.6% strain respectively. When a further load is applied in tension after the interruption at 0.6% strain, it has to overcome extra compressive residual strain of ~ 300 με in the {220} grain families before these grains start deforming plastically. In contrast, {220} grain family yielding is promoted by tensile residual strain when reloading after the interruption at − 0.6% strain. As initiation of macroscopic yielding occurs when these weaker grains start deforming plastically, so the macroscopic yielding will start at a higher applied stress after the interruption at 0.6% strain than the interruption at − 0.6% strain. Conversely, in the case of tension interruptions, the compressive residual strains in the {220} grain families oppose macroscopic yielding. For example, in Fig. 5(b), upon unloading after the interruption at 0.8% strain, the {220} grain family possesses a compressive residual strain of ~ 500 με compared with negligible residual strains upon interruption at − 0.6% strain. When the further load is applied in tension at these two points, less stress is required to deform the {220} grain families plastically after − 0.6% strain interruption than the 0.8% strain interruption. Therefore, macroscopic yielding starts at a higher applied stress after the interruption at 0.8% strain than at − 0.6% strain, as shown in Fig. 3.

It is possible for other stronger grain families to yield before the weaker {220} grain family when they possess high tensile residual strain and the weaker grains possess high compressive residual strain, again as shown in the schematic for 1% tension interruption in Fig. 5(c). Nevertheless, as the residual strains must balance each other, larger tensile residual strains in stronger grains must be matched by increased compressive residual strains in the weaker grain families which decreases the macroscopic yield stress, and vice versa.

4.2. Elastic to plastic transition

Another interesting observation from Fig. 5(c) is that the difference in the macroscopic stress at which the 3 grain families yield also depends upon the magnitude and direction of residual lattice strains in the grain families. For example, in Fig. 5(c), the difference in yield stress between the weaker {220} and the stronger {200} grain family is much higher for − 1% compression interruptions than 0.6% compression interruptions and likewise for − 0.6% tension interruptions compared with 1% tension interruptions. The higher difference between the yield stresses of the grain families means that the macroscopic elastic to plastic transition will occur over a wider range of stresses and vice versa for the lower difference. In other words, if the weaker grains have an increasing tensile residual strain and the stronger grains have an increasing compressive residual strain, the transition from elastic to plastic deformation will take place over a decreasing range of applied stress; that is the shape of the stress-strain curve for elastic to plastic transition will be sharper. Fig. 6 shows an example of such changes in the shape of the macroscopic yield curve with increasing tension interruption strains. Tensile residual strains in the stronger grain families and compressive residual strains in the weaker grain families increases with increasing tension interruptions, therefore, the shape of the stress-strain curve during tensile reloading is observed to be sharper with this increase of interruption strains.

Fig. 7 compares shapes of macroscopic elastic to plastic deformation transition curves for interruptions after which the grain family has relatively similar and different yield stresses. In Fig. 7(a) after − 0.6% compression interruption, the weaker {220} grain family has tensile residual strain and the stronger {200} grain family has compressive residual strain, therefore, the relative tensile yield stress of all the grain

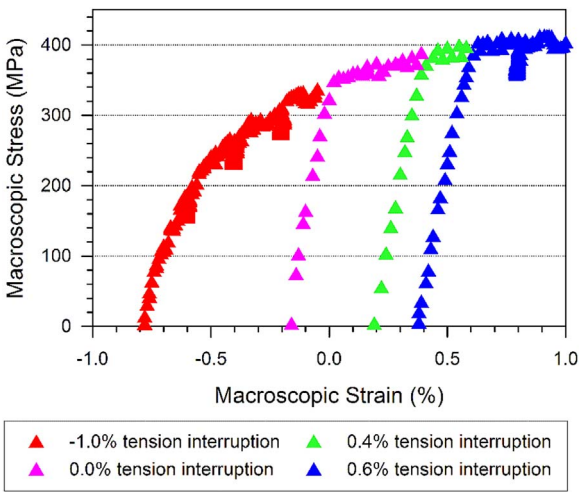

Fig. 6. Macroscopic yielding after interruptions at various strains under tension. The 'elastic to plastic transition zone' gets sharper with an interruption at increasing tensile strain.

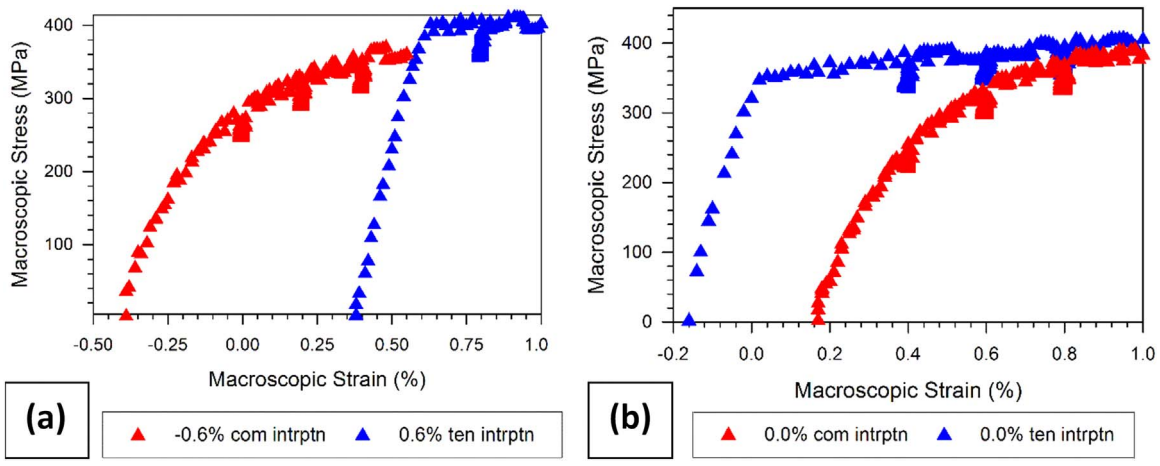

Fig. 7. Comparison of the shapes of macroscopic yield curves after interruptions at (a) 0.6% compression and tension strain and (b) 0.0% compression and tension strain.

families is further apart, while the opposite is the case after interruption at 0.6% tension interruption. Therefore, the macroscopic yield transition curve is much sharper after the 0.6% tension interruption than that after the − 0.6% compression interruption. A similar observation can be made for the example Fig. 7(b) that compares yield deformation transition curves after 0% compression and 0% tension interruptions.

5. Compression yield test

This test mirrored the tensile yield test, investigating the evolution of compressive yield instead of tensile yield, following the same experimental procedure. The tension and compression interruption points for this test are shown in Fig. 1(b). The results are presented concisely in order to avoid repetitiveness.

The measured values of the macroscopic compressive yield stress as a function of the tension and compression interruption points are listed in Table 2 and presented in Fig. 8. Similarly but in an opposite sense to the tensile yield test, the macroscopic compressive yield stress in the subsequent cycle was observed to decrease with increase in the excursion of tensile deformation and to increase with an increase in the excursion of compressive deformation.

Fig. 9(a) and Fig. 9(b) show the evolution of axial residual lattice strains in the 3 grain families after tension and compression interruptions respectively. A similar picture of the evolution of residual lattice strain (but in an opposite sense) can be observed in this test. With increasing tension interruption strains, the residual lattice strain in the plastically weaker {220} grain family increases in compression and that in the {200} grain family increases in tension. On the other hand, with increasing compression interruption strains, the residual lattice strain in the {220} grain family increases in tension and that in the {200} grain family increases in compression. The residual lattice strains in the {311} grain families, remain nearly unchanged in most of the points but show non-systematic fluctuations at a few points.

In contrast to the tensile yield test, the applied stress has to overcome the tensile residual lattice strains in the {220} grain families, to initiate plastic deformation in the macroscopic material. As a result, the macroscopic compressive yield stress will be greater after higher compression interruption strains and lower after higher tensile interruption strains; the exact behaviour can be observed in the variation of macroscopic yield stress with respect to the interruption strains, as presented in Fig. 8.

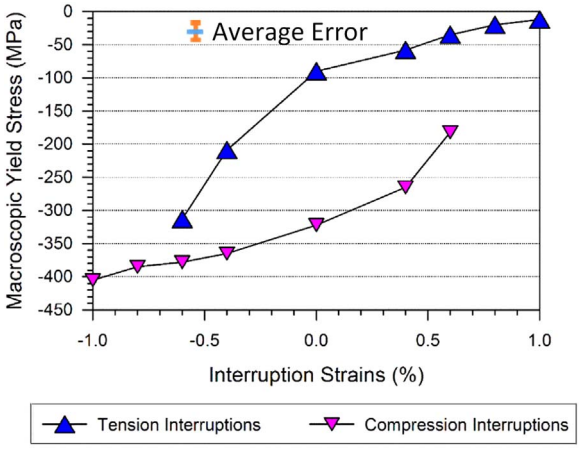

Fig. 8. Changes of cyclic compressive yield stress at 0.05% strain offset after reloading from various tensile and compressive load interruptions. The yield stresses decrease with increasing interruption in tension and increase with the increasing interruption in compression.

Similar observations regarding the changing shape of the macroscopic stress-strain curve were also observed for compression yield test (not presented here). However, contrary to the tension yield test, the macroscopic stress-strain curve for the compression reloading cycle was smoother with increasing tension interruptions, as the lattice yield stress for the stronger grain family is decreasing and that for the weaker

Table 2
Measured yield at 0.0005 strain offset in the reloading cycle after load interruption at various points in compression and tension loading for the compression yield test. The points of the interruption are referred to in Fig. 1.

Compression interruption points	**O**	**P**	**Q**	**R**	**S**	**T**	**U**
Interruption strain (%)	− 0.60	− 0.40	0.0	0.4	0.6	0.8	1.0
Yield at 0.05% strain offset (MPa)	− 313	− 209	− 90	− 58	− 35	− 20	− 12
Tension interruption points	**V**	**W**	**X**	**Y**	**Z**	**AA**	**AB**
Interruption strain (%)	0.6	0.4	0.0	− 0.4	− 0.6	− 0.8	− 1.0
Yield at 0.05% strain offset (MPa)	− 182	− 265	− 322	− 365	− 378	− 385	− 405

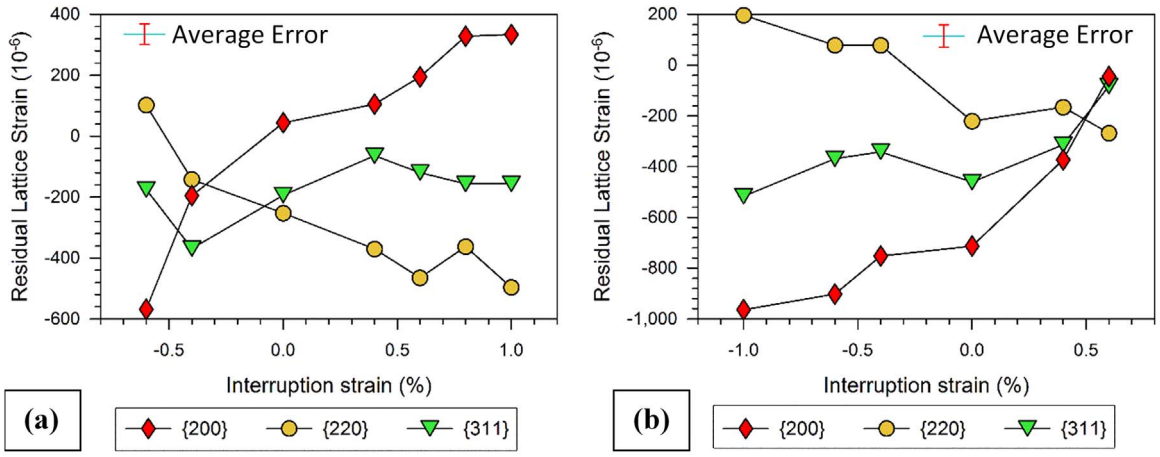

Fig. 9. (a) Lattice residual strains at 5 MPa after interruption at various strains in compressive loading (points N–T in Fig. 1) and (b) lattice residual strains at 5 MPa after interruption at various strains in tensile loading (points O–AB in Fig. 1).

grain family is increasing.

In summary, the above-discussed results of the tensile yield test and compressive yield test show that the changes of microscopic yield stress during a reverse cycle of loading occurs due to the distribution of the forward loading generated residual lattice strains in the grains. Moreover, the changes in the shape of elastic to plastic transition part of the stress-strain curve during tension and compression reloading cycle are also due to the distribution of the residual lattice strains among the grain families.

6. Variation of peak stress and peak lattice strain

The correlation between the evolution of residual lattice strains and macroscopic deformation can be confirmed by examining the variation of macroscopic stress and residual lattice strain at the cycle peak point with respect to the interruption strains. Fig. 10 shows the macroscopic stress (a) at the peak tensile strain of 1% and (b) at the peak compressive strain of − 1% with respect to various tension and compression interruptions. In both cases, the macroscopic stress is seen to be independent of tension, or compression, interruption strain. The small difference between macroscopic stresses after compression interruptions compared with tension interruptions is owing to a slight change in isotropic hardening of the specimen with repeated cyclic loading in the tests.

Fig. 11 shows the evolution of axial residual lattice strains in the three grain families with respect to various interruption strains. Whether the residual lattice strain in a grain family is compressive or tensile in the unloaded state, upon reaching the peak macroscopic tensile strain it has reached the same magnitude. It can be clearly noticed that similar to the macroscopic variation of peak stress, the residual lattice strains in all three grain families remain nearly unchanged irrespective of the interruption strain, except at a few arbitrary points. Thus, a strong correlation can be inferred between the residual lattice strains and the macroscopic stress at the peak 1% tension and peak 1% compression strain points of cyclic loading.

Fig. 11 also shows that the magnitude of the lattice residual strains in any specific grain family is similar after tensile and compressive interruptions in the tension and compression yield tests. This evidence provides added confidence in the precision and consistency of the collected data.

7. Conclusions

Two load interrupted cyclic stress-strain tests were conducted using type 316H austenitic stainless steel samples at room temperature with in-situ neutron diffraction monitoring in order to elucidate the role of residual lattice strain in causing the Bauschinger effect in this material. The following conclusions were drawn from analysis and assessment of the experimental results.

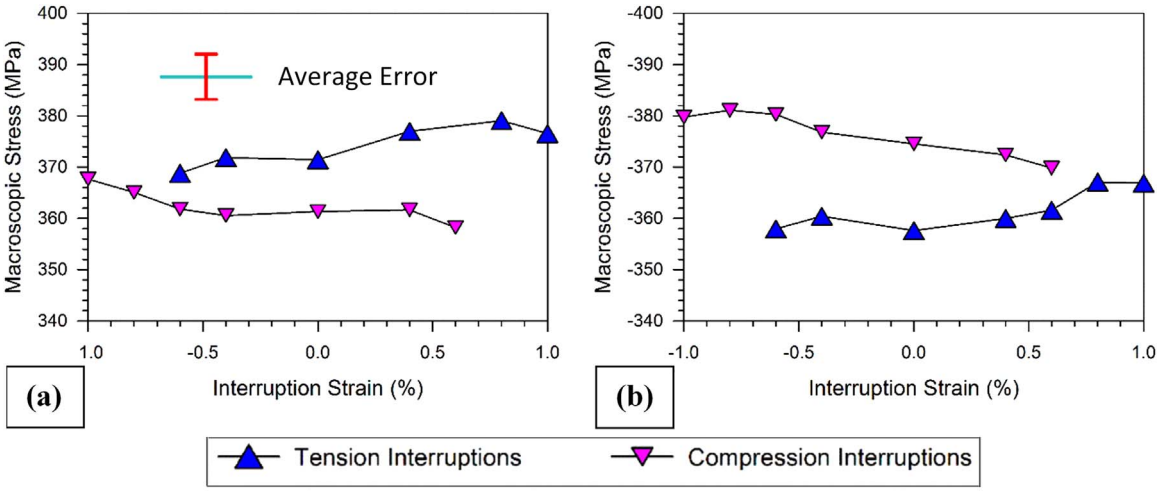

Fig. 10. Macroscopic stress required to reach to the peak 1% tensile strain after the interruption at various compression and tensile loads. The set of macroscopic stress values for both tension and compression interruptions show negligible variations (within experimental error) with interruption strain.

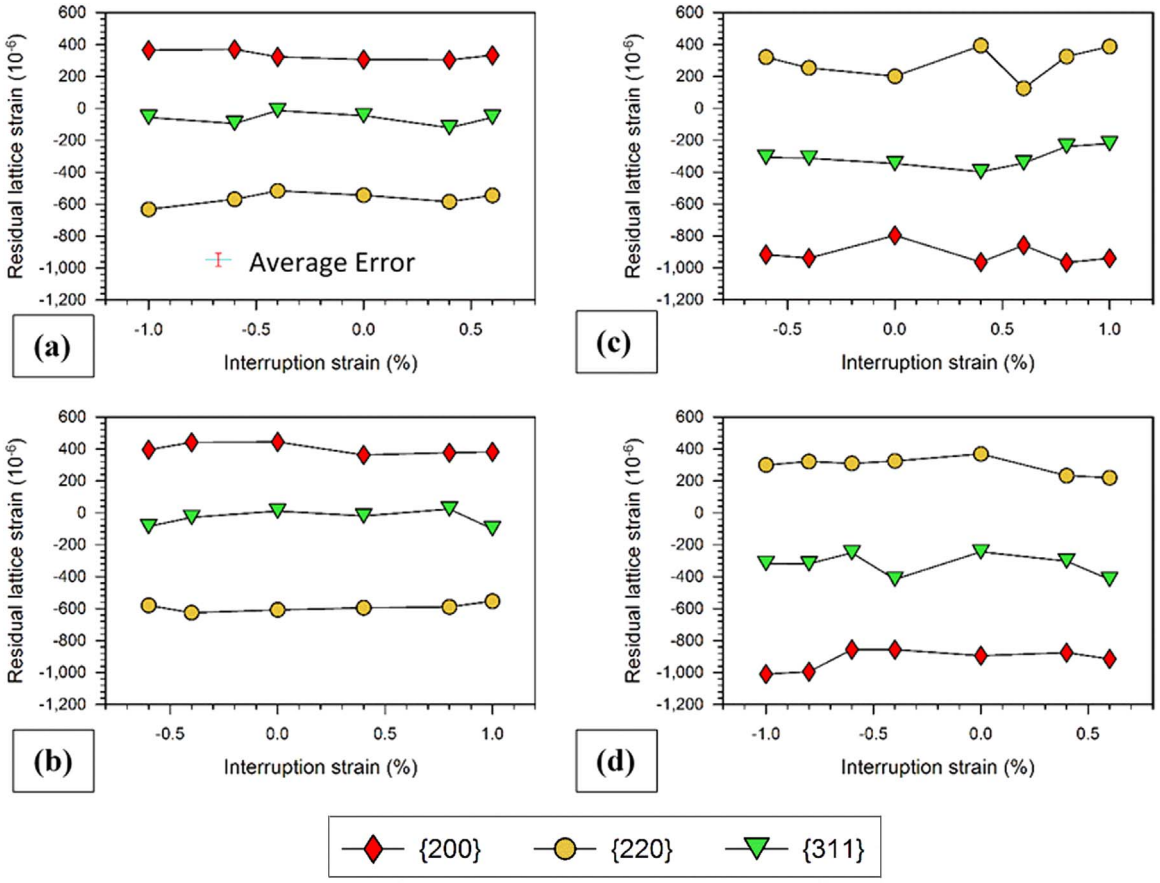

Fig. 11. Variation of axial residual lattice strains after reaching the loop peak strain of 1% after (a) compressive and (b) tensile interruptions in the tension yield test and after (c) tensile and (d) compressive interruptions in the compression yield test.

1. A systematic variation in the magnitude of the yield stress and shape of the stress-strain curve (in tension and compression) was observed on reloading with respect to the magnitude of interruptions under compressive and tensile load. Furthermore, no variation in the macroscopic peak stress was observed owing to load interruptions.
2. It was experimentally inferred that initiation of macroscopic yielding in type 316H stainless steel occurs by the yielding of the plastically weaker {220} grain family and therefore, following an interruption, the magnitude and direction of residual lattice strains in these grains dictate the macroscopic yield stress. A strong correlation was observed between the magnitude and direction of residual lattice strain in this grain family with the magnitude of macroscopic yield stress in both the tests.
3. During tension reloading, after tension interruptions, the macroscopic yielding occurred sharply and after compression interruptions yielding occurred smoothly. The change in shape of the macroscopic stress-strain curve was observed to correlate with the magnitude of residual lattice strains in plastically weaker and plastically stronger grain families. In tensile yield test, sharper yielding occurred with decreasing difference between the yield stresses of the grain families due to weaker grain families possessing compressive residual strains whereas the plastically stronger grain families possessing tensile residual strains. Smoother yielding occurred with increasing difference in yield stress between the grain families, due to residual strains of these grain families in opposite sense.
4. The macroscopic (saturation) stress at the cycle peak 1% tensile strain and peak − 1% compressive strain in reloading cycles were observed to remain almost unchanged irrespective of the interruption strains in both the tension yield and compression yield tests respectively. The lattice residual strains were also observed to remain nearly unchanged in all 3 grain families, irrespective of the interruption strains, at the cycle peaks.

The relationship between macroscopic yielding and microscopic residual lattice strain has been investigated upon reloading after interruptions at various tensile and compressive loads. A strong correlation has been observed between the evolution of residual lattice strain and macroscopic deformation including the cyclic yield stress and shape of the stress-strain curve at yield. This implies that residual lattice strain generated due to grain scale anisotropic elastic and plastic deformation is the primary source of the Bauschinger kinematic hardening effect observed in type 316H austenitic stainless steel.

Acknowledgements

We would like to acknowledge the funding for this research work from EDF Energy Nuclear Generation Ltd, UK. Abdullah Al Mamun is grateful to the Open University for accommodating his Ph.D. studentship. We would also like to thank the STFC ISIS facility for the award of the neutron beam time and funding for conducting the experiment.

References

[1] J. Bauschinger. Mittheilung XV: on the changes of the elastic limit and the strength of iron by straining in tension and in compression, in: Mittheilungen aus dem Mechanisch-Technischen Laboboratorium der Koniglichen Technischen Hochschule in Munchen, 13, 1886, pp. 1–115.
[2] R.P. Skelton, Bauschinger yield in the range 400–1025 °C during cyclic deformation of high temperature alloys, Mater. High Temp. 30 (2013) 241–260.
[3] M.P. O'Donnell, B.S.K., I. Bretherton, D.N. Gladwin, J.P. Hayes, Use of conventional stress-strain data to develop parameters for an advanced constitutive model, Mater.

High Temp. 19 (2002) 215–223.
[4] R.E. Stoltz, R.M. Pelloux, The Bauschinger effect in precipitation strengthened aluminum alloys, Metall. Mater. Trans. 7 (1976) 1295–1306.
[5] A.R. Setoodeh, H. Attariani, Nanoscale simulations of Bauschinger effects on a nickel nanowire, Mater. Lett. 62 (2008) 4266–4268.
[6] A.A. Saleh, E.V. Pereloma, B. Clausen, D.W. Brown, C.N. Tome´, A.A. Gazder, On the evolution and modelling of lattice strains during the cyclic loading of TWIP steel, Acta Mater. 61 (2013) 5247–5262.
[7] M.C. Mataya, M.J. Carr, The Bauschinger effect in a nitrogen-strengthened austenitic stainless steel, Mater. Sci. Eng. 57 (1983) 205–222.
[8] H. Schwartzbart, M.H. Jones, W.F.B. Jr, Observations on Bauschinger Effect in Copper and Brass, National Advisory Committee for Aeronautics, Washington, 1951.
[9] H. Xiaoyu, W. Chao, H. Margolin, S. Nourbakhsh, The Bauschinger effect and the stresses in a strained single crystal, Scr. Metall. Mater. 27 (1992) 865–870.
[10] D.E. Orowan, International Conference on Stresses and Fatigue in Metals, Elsevier, Amsterdam, 1959, pp. 59–80.
[11] A.W. Sleeswyk, M.R. James, D.H. Plantinga, W.S.T. Maathuis, Acta Metall. 26 (1978) 1265–1271.
[12] H. Mughrabi, Dislocation wall and cell structures and long-range internal stresses in deformed metal crystals, Acta Mater. 31 (1983) 1367–1379.
[13] T. Ungar, H. Mughrabi, D. Ronnpagel, M. Wilkens, X-ray line-broadening study of the dislocation cell structure in deformed [001]-orientated copper single crystals, Acta Mater. 32 (1984) 333–342.
[14] F.R.N. Nabarro, Work hardening and dynamical recovery of F.C.C. metals in multiple glide, Acta Mater. 37 (1989) 1521–1546.
[15] A.S. Argon, P. Haasen, A new mechanism of work hardening in the late stages of large strain plastic flow in f.c.c. and diamond cubic crystals, Acta Mater. 41 (1993) 3289–3306.
[16] E.F. Rauch, J.H. Schmitt, Dislocation substructures in mild steel deformed in simple shear, Mater. Sci. Eng.: A 113 (1989) 441–448.
[17] T. Hasegawa, T. Yako, U.F. Kocks, Forward and reverse rearrangements of dislocations in tangled walls, Mater. Sci. Eng. 81 (1986) 189–199.
[18] D.V. Wilson, P.S. Bate, Influences of cell walls and grain boundaries on transient responses of an if steel to changes in strain path, Acta Metall. Mater. 42 (1994) 1099–1111.
[19] E.V. Nesterova, B. Bacroix, C. Teodosiu, Experimental observation of microstructure evolution under strain-path changes in low-carbon IF steel, Mater. Sci. Eng.: A 309–310 (2001) 495–499.
[20] E.F. Rauch, J.J. Gracio, F. Barlat, Work-hardening model for polycrystalline metals under strain reversal at large strains, Acta Mater. 55 (2007) 2939–2948.
[21] Y. Strauven, E. Aernoudt, Directional strain softening in ferritic steel, Acta Metall. 35 (1987) 1029–1036.
[22] B. Peeters, M. Seefeldt, C. Teodosiu, S.R. Kalidindi, P.V. Houtte, E. Aernoudt, Work-hardening/softening behaviour of b.c.c. polycrystals during changing strain paths: I. An integrated model based on substructure and texture evolution, and its prediction of the stress-strain behaviour of an IF steel during two-stage strain paths, Acta Mater. 49 (2001) 1607–1619.
[23] S. Bouvier, J.L. Alves, M.C. Oliveira, L.F. Menezes, Modelling of anisotropic work-hardening behaviour of metallic materials subjected to strain-path changes, Comput. Mater. Sci. 32 (2005) 301–315.
[24] S. Thuillier, E.F. Rauch, Development of microbands in mild steel during cross loading, Acta Metall. Mater. 42 (1994) 1973–1983.
[25] T. Hasegawa, T. Yakou, S. Karashima, Deformation behaviour and dislocation structures upon stress reversal in polycrystalline aluminium, Mater. Sci. Eng. 20 (1975) 267–276.
[26] U.F. Kocks, T. Hasegawa, R.O. Scattergood, On the origin of cell walls and of lattice misorientations during deformation, Scr. Metall. 14 (1980) 449–454.
[27] M.E. Kassner, A.A. Ziaai-Moayyed, A.K. Miller, Metall. Trans. A 16 (1985) 1069–1076.
[28] M.E. Kassner, M.A. Wall, Metall. Mater. Trans. 30 (1999).
[29] M.E. Kassner, M.A. Delos-Reyes, M.A. Wall, Microstructure and mechanisms of cyclic deformation of aluminum single crystals at 77 K, Metall. Mater. Trans 28A (1997) 595–609.
[30] G. Vincze, E.F. Rauch, J.J. Gracio, F. Barlat, A.B. Lopes, A comparison of the mechanical behaviour of an AA1050 and a low carbon steel deformed upon strain reversal, Acta Mater. 53 (2005) 1005–1013.
[31] E.F. Rauch, The stresses and work-hardening rates of mild-steel with different dislocation patterns, Mater. Sci. Eng. A 234 (1997) 653–656.
[32] B. Chen, J.N. Hu, Y.Q. Wang, S.Y. Zhang, S.V. Petegem, A.C.F. Cocks, D.J. Smith, P.E.J. Flewitt, Role of the misfit stress between grains in the Bauschinger effect for a polycrystalline material, Acta Mater. 85 (2015) 229–242.
[33] J.A. Wollmershauser, B. Clausen, S.R. Agnew, A slip system-based kinematic hardening model application to in situ neutron diffraction of cyclic deformation of austenitic stainless steel, Int. J. Fatigue 36 (2012) 181–193.
[34] J. Hu, B. Chen, D.J. Smith, P.E.J. Flewitt, A.C.F. Cocks, On the evaluation of the Bauschinger effect in an austenitic stainless steel—the role of multi-scale residual stresses, Int. J. Plast. 84 (2016) 203–223.
[35] E. Heyn, Internal strains in cold-wrought metals and some troubles caused thereby, J. Inst. Met. 12 (1914) 3–37.
[36] W.A. Wood, N. Dewsnap, Internal stresses in metals, Nature 161 (1948) 617–628.
[37] M.T. Hutchings, P.J. Withers, T.M. Holden, T. Lorentzen, Introduction to the Characterisation of Residual Stresses by Neutron Diffraction, Taylor & Francis, London, 2005.
[38] J.R. Santisteban, M.R. Daymond, J.A. James, L. Edwards, ENGIN-X: a third-generation neutron strain scanner, J. Appl. Crystallogr. 39 (2006) 812–825.
[39] A.A. Mamun, Origin of Creep-Fatigue Back Stress and its Effect on Deformation and Damage. Engineering and Innovation, Vol. Doctor of Philosophy, The Open University, Milton Keynes, UK, 2017.
[40] M.R. Daymond, C.N. Tome, M.A.M. Bourke, Measured and predicted intergranular strains in textured austenitic steel, Acta Mater. 48 (2000) 553–564.
[41] E.C. Oliver, M.R. Daymond, P.J. Withers, Interphase and intergranular stress generation in carbon steels, Acta Mater. 52 (2004) 1937–1951.
[42] M.R. Daymond, Pj Bouchard, Elastoplastic deformation of 316 stainless steel Under tensile loading at elevated temperatures, Metall. Mater. Trans. A 37 (2006) 1863–1873.